

Impact of Drug Conjugation on Thermal and Metabolic Stabilities of Aglycosylated and *N*-Glycosylated Antibodies

Sayumi Yamazoe,* Srikanth Kotapati, Jason M. Hogan, Sean M. West, Xiaodi A. Deng, SJ Diong, Jaren Arbanas, Thien Anh Nguyen, Aarti Jashnani, Diksha Gupta, Arvind Rajpal, Gavin Dollinger, and Pavel Strop*



Cite This: *Bioconjugate Chem.* 2022, 33, 576–585



Read Online

ACCESS |



Metrics & More

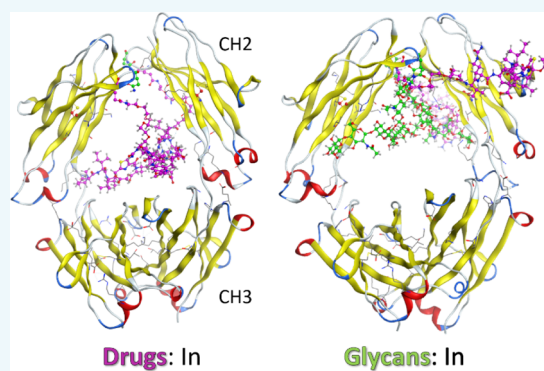


Article Recommendations



Supporting Information

ABSTRACT: N-linked glycosylation is one of the most common and complex posttranslational modifications that govern the biological functions and physicochemical properties of therapeutic antibodies. We evaluated thermal and metabolic stabilities of antibody–drug conjugates (ADCs) with payloads attached to the C'E loop in the immunoglobulin G (IgG) Fc CH2 domain, comparing the glycosylated and aglycosylated Fc ADC variants. Our study revealed that introduction of small-molecule drugs into an aglycosylated antibody can compensate for thermal destabilization originating from structural distortions caused by elimination of N-linked glycans. Depending on the conjugation site, glycans had both positive and negative effects on plasma stability of ADCs. The findings highlight the importance of consideration for selection of conjugation site to achieve desirable physicochemical properties and plasma stability.



INTRODUCTION

Arming monoclonal antibodies (mAbs) with small-molecule drugs enables targeted delivery of a biologically active payload to specific cells expressing target antigen. Antibody–drug conjugates (ADCs) have emerged as a powerful therapeutic modality to specifically eradicate target tumor cells by directing the highly potent cytotoxic drugs to the cells that express specific antigens on their surface. Furthermore, the ADC field is growing beyond oncology therapeutics. For instance, antibody–antibiotic conjugates, which consist of an anti-microbial antibody and a highly efficacious antibiotic, have been developed to treat bacterial infections.¹ ADCs have also been utilized to deliver antigens, adjuvants, or innate agonists to the tumor micro-environment or to antigen-presenting cells to boost immune response specific to malignancies.^{2,3} To date, a total of twelve ADCs have been approved by the FDA and the indications include various hematological malignancies as well as solid tumors. Although ADCs have great potential to make a paradigm shift in targeted therapy, designing an ideal ADC is complex, as attaching a hydrophobic payload can lead to structural destabilization and enhanced propensity to aggregate.⁴ Generally, coupling the drug to the antibody results in a decrease in melting point, and the negative impact on thermal stability is intensified with increased drug loading and hydrophobicity of payload.⁵ In addition to thermodynamic properties, metabolic and chemical stability of the payload and specific cleavability of the linker also need to be considered. The payload should be stable during storage and circulation in the

blood and also efficient release of free payload is required at targeted sites. The stability of payload is highly dependent on the conjugation site that has diverse electrostatic and/or steric environments. In this work, we evaluated thermodynamic properties and plasma stability of site-specific ADCs bearing the linker-payload in close proximity to the CH2 C'E loop Asn297 undergoing *N*-glycosylation, which plays a critical role in thermal stability of antibody therapeutics.

To our surprise, an improvement in the melting temperature was observed by introducing a tubulysin payload to aglycosylated antibodies. The two opposing CH3 domains form extensive hydrophobic interactions that involve more than 20 residues per chain. In contrast, the interaction between the opposing CH2 domains is principally through the conserved *N*-glycans attached at Asn297, which project along the inner surface of the CH2 domains and occupy the interstitial space between domains.⁶ We hypothesized that in the absence of glycans, payload can occupy the inter-chain cavity and provide stabilizing interactions to the CH2 domain as well as protect linker-payload. The feasibility of this “drug-in” conformation is

Received: December 4, 2021

Revised: February 10, 2022

Published: March 28, 2022



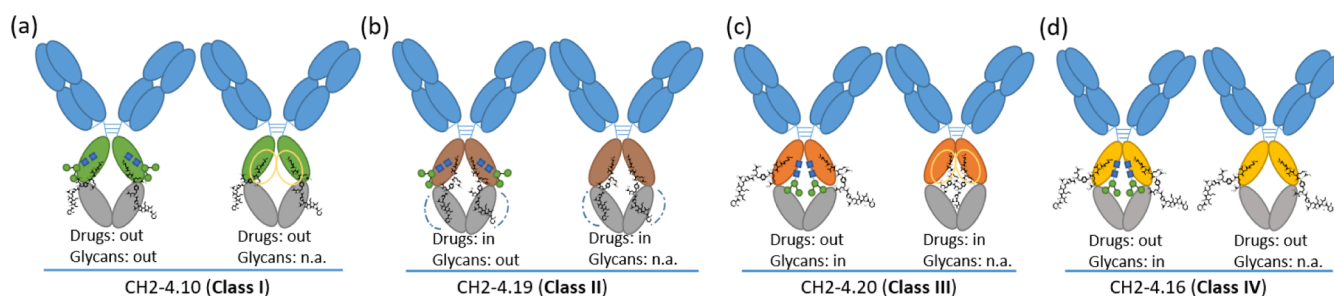


Figure 1. Illustration of ADCs in the presence or absence of glycosylation. (a) Drugs are incapable of filling the interstitial space regardless of *N*-glycosylations. (b) *N*-glycans are projected to solvent exposed regions, whereas drugs undergo slow deacetylation. (c) *N*-glycans are buried between the two Fc chains. The attached drugs are unable to replace glycans stably positioned in the cavity created by the CH2–CH3 chains. In the absence of glycans, the drugs are capable of occupying the inter-domain pocket. (d) Drugs are exposed outward, whereas oligosaccharides fit between the two Fc chains.

also supported by the molecular model (Supporting Information Figure S1).

To explore this hypothesis, we introduced the drug to different locations within the C'E loop and measured the thermal characteristics of the antibodies, glycan heterogeneity, and metabolic stability in the presence and absence of glycans. Throughout the analysis, we assumed four potential modalities (Figure 1a–d): (1) neither *N*-glycan nor payload fills the interstitial space between CH2 domains; (2) glycans are exposed, whereas drugs are protected regardless of glycan status; (3) glycans are stably buried between CH2 chains, decreasing access of drugs to the inter-chain cavity, but drugs acquire access to the inter-chain space in the absence of glycans; and (4) glycans are buried between the two Fc chains, whereas drugs are incapable of occupying the inter-domain cavity even in the absence of glycans. Our data identified the complex relationship between the conjugation site, glycan position, ADC stability, and ADC melting temperature. These parameters govern overall ADC stability and should be considered when designing drug conjugation sites near the location of Fc glycosylation.

RESULTS AND DISCUSSION

Conventional ADCs use random conjugation technologies, which utilize reactive functional groups within naturally occurring amino acids such as lysines or inter-chain disulfide cysteines.⁷ These technologies can result in a heterogeneous mixture of ADCs containing varying drug load or distribution and each with distinct pharmacokinetic, efficacy, and thermodynamic properties. Upon lysine or cysteine linking of payloads, protein conformation is not considerably altered and typically the capability to recognize an antigen is preserved. However, the conformational energy of unfolding is decreased, and a more hydrophobic local surface is created. Correspondingly, the melting temperatures can decrease, increasing the propensity to aggregate. Molecules with higher drug-to-antibody ratios (DARs) are more prone to aggregation and display detrimental impacts on thermal stability.⁵ The destabilization of the CH2 domain upon conjugation to the surface lysines or reduced inter-chain disulfides is the major contribution to the loss of higher-order structure through unfolding as evidenced by disruption of thermal conformational integrity. The melting temperature of the CH2 domain is more influenced by drug conjugation compared to the Fab/CH3 domain.⁸

Site-specific conjugation technologies intrinsically exhibit only minor or negligible distribution of positional isomers. Strategies include the incorporation of additional unpaired

cysteine residues or non-natural amino acids that can be used as a handle to introduce appropriately functionalized linker payloads.^{9–12} Engineered peptide tags are an alternative approach that enables enzyme-mediated bioconjugation.¹² To date, few studies have been published regarding the influence of site-specific conjugation approaches on structural stability. As anticipated, thermal stability and resistance toward proteolysis was shown to be highly dependent on the site of conjugation.¹³ Except for a recently published engineered strain¹⁴ or using positively charged oligopeptide linkers (WO2019057772A1), bacterial transglutaminase (bTGase)-mediated conjugation to the endogenous Gln295 residue requires prior deglycosylation or engineering to expose the recognition sequence near the native *N*-glycosylation site at Asn297. The removal of carbohydrate chains from IgG molecules promotes significant conformational changes manifested by increased susceptibility of deglycosylated and aglycosylated antibodies to proteases and decreased thermal stability of antibodies.¹⁵ Location of the conjugation site has been demonstrated to have an impact not only on the conformational integrity but also on the stability of linker and payload. A number of studies revealed that the selection of positions for conjugation has a considerable influence on the chemical and metabolic stabilities of the linkage within the tethered drug, which could dominate in vivo pharmacokinetics.^{12,16} Therefore, we decided to conduct a detailed study on the effects of site-specific drug loading on thermal characteristics and plasma stability of the resulting ADC, in relation to conserved *N*-glycans in the CH2 domain.

Site-specific ADCs were generated by microbial transglutaminase (bTGase) that catalyzes the covalent cross-linking of glutamine and lysine-containing peptides or proteins by formation of an isopeptide bond. Though bTGase has low substrate specificity and can therefore accept a wide range of lysine-containing entities, the enzyme is more selective toward the glutamine residues. Both protein chain flexibility and neighboring amino acids affect bTGase-mediated conjugation efficiency. Antibodies generally lack such a site and are not efficiently modifiable by bTGase. However, after removal of the carbohydrate moiety, a unique site is exposed that permits conjugating precisely one substrate to each heavy chain at amino acid Gln295.¹⁷ By site-directed point mutagenesis, it is possible to install an additional Gln residue at position 297 which can then accommodate a second substrate per heavy chain, thereby generating homogeneous ADCs with DAR 4. Another approach to introduce drug linkers into glycosylated antibodies with bTGase is to insert short peptide motifs containing glutamine into the antibody sequence. This strategy is particularly valuable

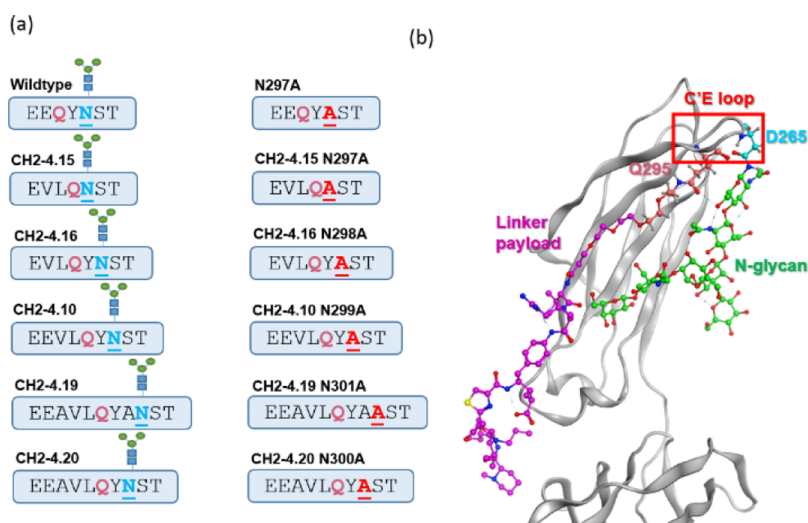


Figure 2. Genetic variants containing a conjugatable glutamine residue within three residues from an *N*-glycosylation site. (a) Sequence of insertion to introduce to the C'E loop to enable bTGase-mediated conjugation. (b) CH2 domain of mutant CD2-4.16 indicating the position of an acceptor glutamine (Q295) and glycosylation site asparagine (N297).

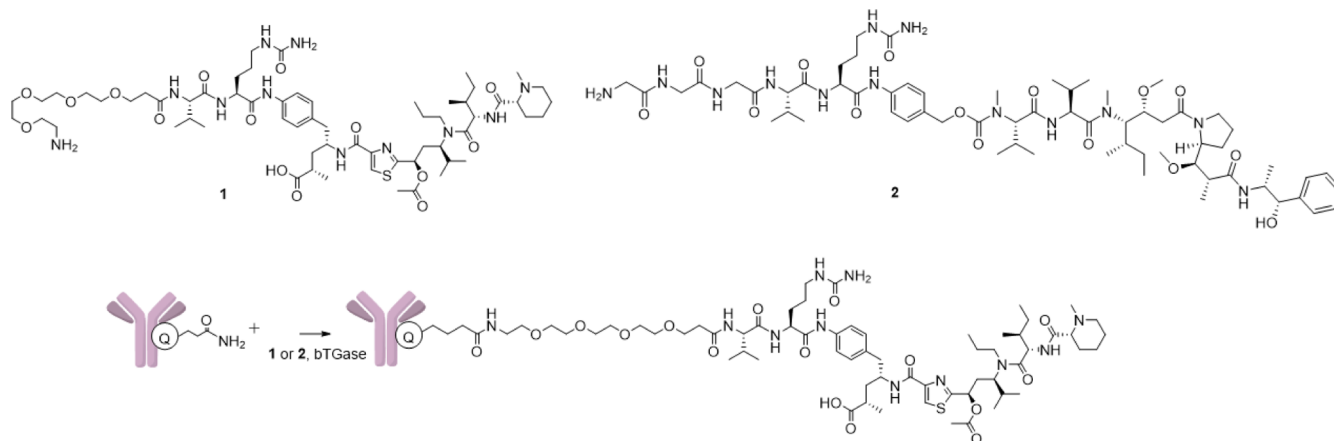


Figure 3. Structures of payload linker used for this study. Amine-functionalized tubulysin (1) or Gly3 MMAE (2) was reacted with antibodies in the presence of bTGase in 20 mM Tris pH 8 buffer.

Table 1. Genetic Variants with Engineered Glutamine Tags for bTGase Conjugation

| variant | residue no. of Q | Q position relative to N | insertion sequence from E293 | DAR with tubulysin (1) | aggregates of ADC |
|----------------|------------------|--------------------------|------------------------------|------------------------|-------------------|
| wildtype | 295 | N-2 | EEQYNST | n.d. | n.d. |
| N297A | 295 | n.a. | EEQYAST | 1.8 | 4% |
| CH2-4.15 | 296 | N-1 | EVLQNST | 2.0 | <1% |
| CH2-4.15 N297A | 296 | n.a. | EVLQAST | 2.0 | 5% |
| CH2-4.16 | 296 | N-2 | EVLQYNST | 2.0 | <1% |
| CH2-4.16 N298A | 296 | n.a. | EVLQYAST | 1.9 | 4% |
| CH2-4.10 | 297 | N-2 | EEVLQYNST | 1.9 | <1% |
| CH2-4.10 N299A | 297 | n.a. | EEVLQYAST | 2.0 | 4% |
| CH2-4.19 | 298 | N-3 | EEAVLQYANST | 2.0 | 11% |
| CH2-4.19 N301A | 298 | n.a. | EEAVLQYAAST | 2.0 | 4% |
| CH2-4.20 | 298 | N-2 | EEAVLQYNST | 1.9 | 7% |
| CH2-4.20 N300A | 298 | n.a. | EEAVLQYAST | 1.9 | 4% |

when it is desirable to preserve effector functions of ADCs. Our recent screening led to the identification of several genetic variants containing the engineered glutamine tag that permits coupling of linker payload into the C'E loop where *N*-glycosylation occurs.¹⁸ Using these constructs, we tested the impact of loading drug linkers on the thermal stability of

glycosylated and aglycosylated antibodies. In general, conjugating the drug to a glycosylated antibody resulted in decreased thermal stability, whereas attaching the drug to an aglycosylated antibody led to an increased melting temperature for some of the constructs.

Glycosylation is a key feature of the Fc region of all IgG subclasses. The CH2 domain contains a single Asn297 side chain extended by *N*-glycan chain in the conserved loop between strands C' and E. For our test, we selected five mutants that contain a conjugatable glutamine residue within three residues from an *N*-glycosylation site (Figure 2). The antibody binding target is mesothelin, a glycosylphosphatidylinositol-anchored membrane protein that shows promise as a target for antibody-directed cancer therapies (sequence shown in the Supporting Information). These mutants (CH2-4.15, CH2-4.16, CH2-4.10, CH2-4.19, and CH2-4.20) were produced by transient transfection in Expi293 cells. Expression yields were found to be highly dependent on mutations and presence/absence of glycans (Supporting Information Table S1). Interestingly, for two genetic variants (CH2-4.16 and CH2-4.10), the removal of glycans significantly improved production yields.

Generated mAbs showed highly efficient conjugation when the antibody was reacted with an amine-functionalized tubulysin analogue (1, Figure 3) in the presence of bTGase containing two point mutations (V65I and Y85F).¹⁹ The ADC produced generally displayed a high monomer content ($\geq 95\%$) with the exception of CH2-4.19 and CH2-4.20 where conjugation resulted in moderate levels of aggregates, 11 and 7%, respectively (Table 1). We then eliminated the *N*-glycosylation site by mutating the conserved asparagine (N) residue within a consensus N–S–T acceptor site into alanine (A) by site-directed mutagenesis to yield aglycosylated versions of the five above listed variants along with the parental antibody containing the same N297A mutation (Table 1). The expressed aglycosylated variants were subjected to bTGase-mediated bioconjugation with amine-tubulysin (1) by adopting the same procedure used for reactions of glycosylated antibodies. These deglycosylated constructs reacted readily with 1 to furnish homogeneous products with DAR close to the theoretical maximum 2 (≥ 1.8).

It has been shown that both *N*-glycosylation and addition of drug affects thermal characteristics of therapeutic antibodies.^{5,20} Thermogram profiles of the parental antibody and conjugated product were assessed by differential scanning calorimetry (DSC). Previous studies have indicated that IgG1 antibodies typically have three thermal transitions in DSC.^{21,22} The first peak with the lowest transition temperature usually represents the thermal transition of the CH2 domain in the Fc region; the second or third peak with the largest peak height corresponds to the thermal transition of the Fab region; and the remaining peak is the contribution of the CH3 domain of the Fc region of the antibody. Elimination of glycans had minimal effects on the thermal transition change for the Fab region and the CH3 domain. However, when the conserved *N*-glycosylation site was replaced with alanine to prevent this posttranslational modification, the transition temperature of the CH2 domain was shifted lower, with associated decrease in the onset temperature T_{onset} , reflecting the first reversible CH2 transition. Indeed, introducing a N297A mutation to the wild-type CH2 sequence resulted in decreases in both thermal onset and unfolding ($T_{\text{m}1}$) temperature of 5.7 and 2.4 °C, respectively. This is consistent with the observation that the removal of *N*-glycans at Asn297 in the heavy chain Fc region causes conformational changes, which leads to decreased thermal stability.²³ Other variants showed similar trends: T_{onset} of aglycosylated antibodies was 3.7–6.6 °C lower compared to the

glycosylated form, which supports the finding about contribution of *N*-glycans to conformational integrity.

Mild destabilization of the CH2 domain was observed when linker payload was conjugated to glycosylated antibodies (Table 2, e.g., CH2.4-16 vs CH2-4.16-tubulysin). Similar observations

Table 2. Comparison of Melting Temperatures of mAbs

| variant name | T_{onset} | $T_{\text{m}1}$ | $T_{\text{m}2}$ | $T_{\text{m}3}$ |
|--------------------------|--------------------|-----------------|-----------------|-----------------|
| wildtype | 64.5 | 67.3 | 71.1 | 82 |
| N297A | 58.8 | 64.9 | 70.5 | 82.1 |
| N297A-tubulysin | 62.7 | 69.1 | 70.8 | 82.3 |
| CH2-4.15 | 64.4 | 69.9 | 71.7 | 82.2 |
| CH2-4.15-tubulysin | 61.8 | 67.4 | 70.4 | 81.4 |
| CH2-4.15 N297A | 59.4 | 66.6 | 70.4 | 82.3 |
| CH2-4.15 N297A-tubulysin | 59.7 | 65.2 | 69.8 | 82.3 |
| CH2-4.16 | 62.7 | 68.4 | 70.6 | 82.1 |
| CH2-4.16-tubulysin | 59.7 | 65.9 | 69.5 | 81.4 |
| CH2-4.16 N298A | 56.4 | 62.2 | 69.8 | 82.1 |
| CH2-4.16 N298A-tubulysin | 56.8 | 65.3 | 69.3 | 81.4 |
| CH2-4.10 | 58 | 64.2 | 69.9 | 81.6 |
| CH2-4.10-tubulysin | 55.7 | 65 | 69.6 | 81.1 |
| CH2-4.10 N299A | 54.3 | 61.2 | 69.7 | 81.9 |
| CH2-4.10 N299A-tubulysin | 60.5 | 65.9 | 70.3 | 82.1 |
| CH2-4.19 | 57 | 64.5 | 70.4 | 81.6 |
| CH2-4.19-tubulysin | 53.9 | 62.9 | 69.3 | 81.5 |
| CH2-4.19 N301A | 52.2 | 59.3 | 69.6 | 81.8 |
| CH2-4.19 N301A-tubulysin | 53.7 | 63.7 | 69.3 | 81.4 |
| CH2-4.20 | 60.8 | 67.9 | 70.6 | 82 |
| CH2-4.20-tubulysin | 56.6 | 64.9 | 69.5 | 81.3 |
| CH2-4.20 N300A | 54.2 | 60.4 | 70 | 82.2 |
| CH2-4.20 N300A-tubulysin | 57.9 | 64.9 | 70.3 | 82.3 |

have been reported for several classes of ADCs in which modification and conjugation of the antibody impacted the thermal stability.⁴ Intriguingly, attaching linker payload to an aglycosylated antibody resulted in no change to the T_{onset} (CH2-4.15, CH2-4.16) or in various degrees of stabilization of the T_{onset} (CH2-4.19, CH2-4.20, and CH2-4.10). The recovery of T_{onset} of the aglycosylated CH2 domain suggests that addition of linker payload can compensate for loss of stability due to glycan elimination in a context-dependent manner. This effect was particularly prominent for two variants, CH2-4.16 and CH2-4.20, displaying ΔT_{onset} of 6.2 and 3.7 °C, respectively (Table 2, Supporting Information Figures S2–S4). In these two mutants, conjugating payload linkers induced a substantial shift in thermal stability which overcomes the decrease of T_{onset} and $T_{\text{m}1}$ due to the loss of *N*-glycosylations.

Next, we tested plasma stability of the generated ADCs. In addition to deconjugation, it has been demonstrated that several classes of ADCs undergo metabolic inactivation such as deacetylation in tubulysin and amide hydrolysis in MMAD, which is impacted by the conjugation site. Deacetylation rates of our tubulysin ADCs were measured by immunocapture liquid chromatography–mass spectrometry (LC–MS) (Figure 4). Ten ADCs bearing the linker payload at different sites were subjected to sub-fragment analysis and stability of the linkage and payload was analyzed by LC–MS.²⁴ In general, introducing payload linker near the CH2 glycosylation site via bTGase provides a considerable stabilizing effect. In fact, the N297A ADC with linked tubulysin attached to Gln295 position showed no deconjugation and a low level of deacetylation (9.8%) over a 5-day period (Table 3). The other nine ADCs with drug linkers

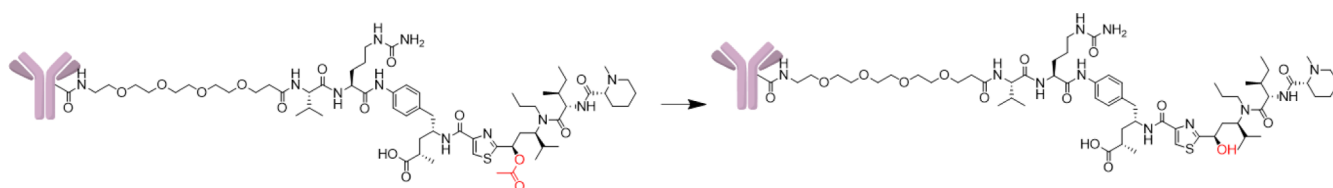


Figure 4. Deacetylation of tubulysin attached to an antibody. Tubulysin deacetylation is caused by mouse serum enzymes and impacts drug linkers conjugated particularly at solvent-exposed positions.

Table 3. Deacetylation Rate of ADCs in Mouse Serum^a

| ADC name | day 1 | day 2 | day 5 |
|--------------------------|-------|-------|-------|
| N297A-tubulysin | 1.35 | 3.01 | 9.85 |
| CH2-4.15-tubulysin | 6.34 | 11.62 | 33.15 |
| CH2-4.15 N297A-tubulysin | n.d.* | n.d.* | n.d.* |
| CH2-4.16-tubulysin | 4.03 | 8.48 | 21.65 |
| CH2-4.16 N298A-tubulysin | 3.6 | 7.92 | 32.39 |
| CH2-4.10-tubulysin | 2.41 | 5.11 | 16.44 |
| CH2-4.10 N299A-tubulysin | 2.73 | 6.63 | 24.68 |
| CH2-4.19-tubulysin | 2.23 | 4.23 | 14.86 |
| CH2-4.10 N301A-tubulysin | 1.71 | 3.31 | 12.64 |
| CH2-4.20-tubulysin | 8.06 | 16.48 | 51.18 |
| CH2-4.10 N300A-tubulysin | 1.72 | 3.56 | 12.27 |

^aPercent deacetylation of tubulysin was measured at 1, 2, and 5 days after incubation of ADCs in mouse serum. % deacetylation is shown.

installed in different positions presented varying rates of deacetylation when incubated at 37 °C in mouse serum, whereas no deconjugation was noted for any of the ADCs. Four pairs of ADCs (CH2-4.16, CH2-4.10, CH2-4.19, and CH2-4.20) with or without *N*-glycans were included in this study. Addition of glycans did not largely affect the serum stability of CH2-4.19 and had a mild effect for CH2-4.10 and CH2-4.16 ADCs. Exceptionally, CH2-4.20 demonstrated significant stabilization of payload when carbohydrate chains were not present. Though CH2-4.20 N300A-tubulysin showed a moderate degree of hydrolysis (12.3%) at day 5, the rate of tubulysin deacetylation was significantly faster when drug was conjugated to the corresponding glycosylated antibody, resulting in 51.2% of deacetylation in 5 days (Table 3).

We tested the thermodynamic properties and plasma stability of ADCs bearing another commonly used linker payload MMAE (2). Eleven ADCs based on genetic variants CH2-4.10, 15, 16, 20, and N297A were produced by bTGase (Supporting Information Table S2). Consistent with what is observed with tubulysin ADCs, enhancement or minor change of T_{onset} was

noted when MMAE linker payload was attached to aglycosylated mAbs (ΔT_{onset} +0.2 to +5.6), whereas thermal destabilization was induced by introduction of linker payload to glycosylated mAbs (ΔT_{onset} −9.8 to −3.0) (Table 4). Mouse plasma stability of 11 ADCs was assessed as well (Supporting Information Table S3). All ADCs showed a minor deconjugation indicating that attaching linker drug to this region via bTGase-mediated conjugation generally provides high plasma stability. In vitro cell killing activity of the generated tubulysin and MMAE ADCs was also assessed using human lung cancer cell line H226 expressing mesothelin (Supporting Information Table S4). Generated site-specific ADCs were functionally active and exhibited subnanomolar potency.

During mass spectrometric characterization, it was noted that CH2 engineered antibodies tended to show a high degree of glycan branching (Supporting Information Figure S4). The composition and patterns of glycoforms could have positive or negative effects on the physicochemical properties and biological functions of therapeutic antibodies. It is well recognized that the absence of *N*-linked glycans abrogates nearly all FcγR-binding affinity and immune effector functions that are critical for clearing antibody-opsonized tumor cells. In order to gain precise insights into the glycan patterns of the expressed antibodies containing the peptide insertion for conjugation near the *N*-glycosylation site, the *N*-glycans linked to each IgG were subjected to structural analysis using quantitative HILIC–LC–MS. Briefly, the glycans were enzymatically released from the antibody, labeled, and analyzed by LC–FLR–MS. We noted that engineering the loop where glycosylation occurs generally increases the heterogeneity of glycoforms (Figure 5a,b and Table S5). For instance, the amount of terminal sialylation in the wild-type antibody was undetectable, whereas a significant amount of sialylated glycans was observed in the engineered proteins. The level of sialylation was remarkably high for CH2-4.10 and CH2-4.19 and terminal sialylation was observed on 16.39 and 17.34% of the total protein, respectively (Figure 5c).

Table 4. Comparison of Melting Temperatures of mAbs and ADCs

| variant name | T_{onset} | $T_{\text{m}1}$ | $T_{\text{m}2}$ | $T_{\text{m}3}$ | $\Delta T_{\text{onset}}^a$ MMAE | $\Delta T_{\text{onset}}^a$ tubulysin |
|---------------------|--------------------|-----------------|-----------------|-----------------|----------------------------------|---------------------------------------|
| N297A-MMAE | 63.5 | 70.5 | 71.9 | 82.3 | +4.7 | +3.9 |
| CH2-4.15-MMAE | 54.6 | 57.0 | 70.7 | 84.1 | −9.8 | −2.6 |
| CH2-4.15 N297A-MMAE | 62.0 | 66.7 | 70.66 | 82.7 | +2.6 | +0.3 |
| CH2-4.16-MMAE | 57.7 | 67.7 | 70.8 | 82.6 | −5.0 | −3.0 |
| CH2-4.16 N298A-MMAE | 56.6 | 66.9 | 70.7 | 82.8 | +0.2 | +0.4 |
| CH2-4.10-MMAE | 54.2 | 63.8 | 70.7 | 82.6 | −3.8 | −2.3 |
| CH2-4.10 N299A-MMAE | 59.7 | 65.8 | 70.7 | 82.9 | +5.4 | +6.2 |
| CH2-4.19-MMAE | 54.0 | 61.2 | 70.6 | 82.6 | −3.0 | −3.1 |
| CH-4.19 N301A-MMAE | 54.3 | 61.5 | 70.5 | 82.8 | +2.1 | +1.5 |
| CH2-4.20-MMAE | 55.2 | 66.8 | 70.8 | 82.7 | −5.6 | −4.2 |
| CH2-4.20 N300A-MMAE | 55.4 | 62.1 | 71.5 | 84.3 | +1.2 | +3.7 |

^aDifference in T_{onset} between the genetic variant and corresponding ADC.

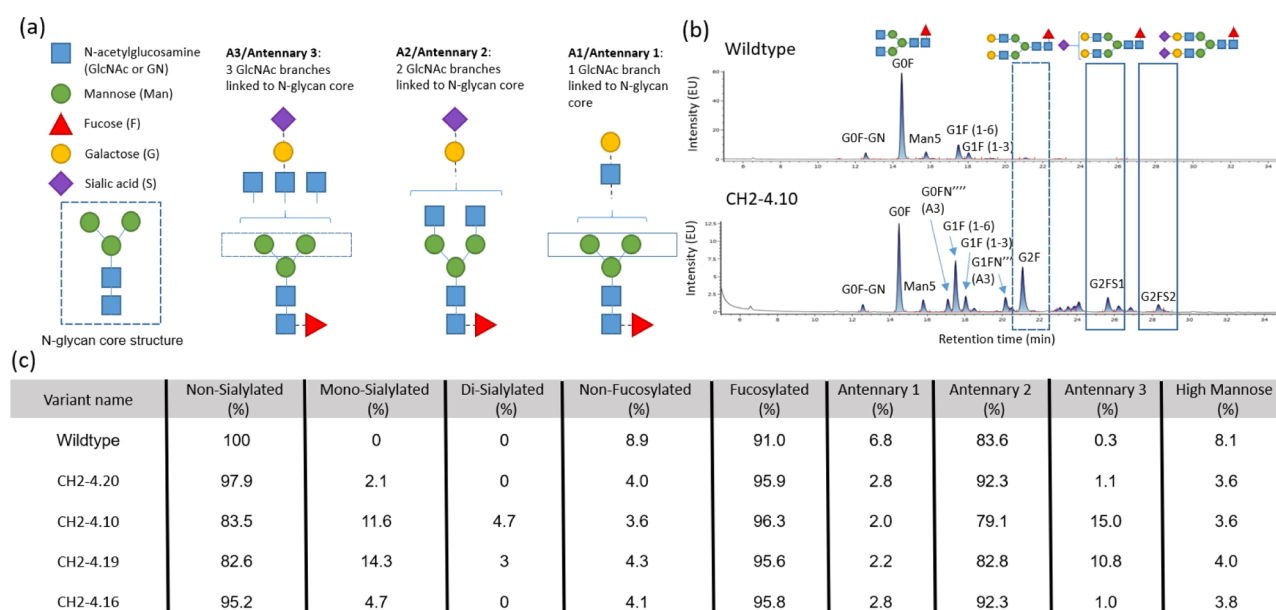


Figure 5. Glycan profile of antibodies with bTGase tag expressed in Expi293. (a) Types of *N*-glycans. The three different types share a common core structure including the first two *N*-acetylglucosamine residues and the first three mannose residues. (b) HPLC–FLD chromatogram of *N*-glycans. (c) Glycan classification summary for each antibody. Engineered antibodies displayed higher degrees of branching and sialylation compared to wildtype. The highest level of tri-antennary glycans was observed for CH2-4.10. *The data for CH2-4.15 N297A ADC was not obtained because of unsuccessful elution from immuno capture possibly due to precipitation during incubation with the plasma or sample preparation process or due to mis-cleavage by IdeS.

Correspondingly, these two variants displayed a greater degree of tri-antennary glycans (10–15%), compared to the wild-type IgG (0.35%). The level of glycan heterogeneity was intermediate in other two variants (CH2-4.20 and CH2-4.16). Several structural features including *N*-acetylglucosamine branching and terminal sialylation are reported to correlate with the solvent accessibility of the glycosylation sites of maturely folded glycoproteins. Antibodies represent a special group of glycoproteins as their carbohydrate chains are of limited size, characterized by scarcity of *N*-glycans with more than two antennae and low sialic acid content, in agreement with our observations. This circumstance is explained by the fact that the Asn297 residue within the CH2 domain is buried in the tertiary structure, where enzymatic conversion or extension of glycans is hampered because of restricted accessibility. A greater degree of glycan heterogeneity found on the engineered antibodies implies elevated regional solvent accessibility of the glycosylation site and glycans. The enhanced diversity of glycans was also associated with decrease of T_{onset} and T_m in our study. The melting temperature was considerably lower for two mutants (CH2-4.10 and CH2-4.19), showing approximately a 7 °C lower T_{onset} compared to wild-type IgG. For other constructs that showed lesser degree of glycan diversity (CH2-4.16 and CH2-4.20), the thermal destabilization effect was less prominent. Glycan analysis was also conducted for antibodies expressed in ExpiCHO that are generally used for commercial production. The study confirmed that the trends such as % tri-antennary, % high mannose, and % fucosylated are conserved between the different expression systems, whereas slightly lower sialylation was observed in these constructs relative to those expressed in Expi293 (Supporting Information Table S6).

We measured the binding affinities of the generated genetic variants and resulting ADCs to Fc γ receptors (Fc γ Rs) by surface plasmon resonance analysis (Supporting Information Table S7). Wild-type human IgG showed expected binding to

Fc γ Rs. Engineering of the CH2 domain for site-specific conjugation did not largely affect the binding affinities, however, a minor negative effect was noted for genetically modified variants that have relatively large insertion such as CH2-4.19 and CH2-4.20. Introduction of payload to the C'E loop was generally well tolerated and ADCs with glycans demonstrated similar levels of binding compared to the parental antibodies. Aglycosylated antibodies showed abrogated binding to the low-affinity receptors regardless of drug attachment. These antibodies and ADCs displayed approximately 100-fold weaker binding to hCD64 compared to the corresponding glycosylated species.

Based on thermodynamic profiling, plasma stability, and glycan patterns, we presumed an intricate connection between glycans and drugs (Figure 1). Drugs can be positioned to solvent-exposed regions regardless of glycans such as CH2-4.10 that shows poor thermal and plasma stability. On the other hand, drugs can be protected both in the presence and absence of glycans as seen for CH2-4.19. Another interesting case is that drugs and glycans compete and payload is exposed outside the CH2 cavity in the presence of glycans. For instance, CH2-4.20 ADC displays poor plasma stability when glycans are attached. It is also possible that drugs fail to occupy the interstitial space between CH2 domains, whereas glycans are projected to fill the space. CH2-4.16 can fall into this last category based on the characteristics observed in our study. To verify the structural hypothesis of solvent-exposed glycans, the PNGase-mediated deglycosylation rate of selected genetic variants and ADC was measured (Supporting Information Figure S6). Native mAb and CH2-4.15 showed slower deglycosylation rates compared to variants with greater glycan diversity. A set of genetic variants bearing the highest degree of carbohydrate diversity (CH2-4.10 and CH2-4.19) underwent the fastest deglycosylation and a general correlation between enzyme-mediated deglycosylation kinetics and glycan diversity was observed. It is noteworthy to

mention that CH2-4.20-tubulysin ADC displayed resistance to PNGase-mediated deglycosylation compared to naked CH2-4.20 supporting the hypothesis of tighter packing of glycans within the CH2 cavity in the presence of tubulysin linker payload.

CONCLUSIONS

The study demonstrated that thermal denaturation and metabolic stability of site-specific ADCs can be altered by engineering of the CH2 domain, N-linked glycans, and location of drugs. In our study, we used the native human IgG1 sequence and engineered variants that enable site-specific introduction of linker payload to different positions of the C'E loop in the presence or absence of N-glycosylation. It was found that generally the insertion of the bTGase tag and shifting the Asn297 position led to more diverse compositions of the glycan structure, probably due to the enhanced accessibility for the appropriate glycotransferases that catalyze chain elongation reactions. In the native IgG1 sequence, the carbohydrates at Asn297 interact with neighboring amino acids on the inner side of the CH2 chain, therefore a hydrophobic patch inside the CH2 domain is masked by the glycan.²⁵ Particularly, it has been known that the side chains of aromatic residues including Phe241 and Phe243 of the Fc domain face the carbohydrates and disrupting these carbohydrate–aromatic interactions destabilizes the CH2 domain.²⁶ When the dynamic motion of glycan chains is intensified, the transient exposure of the hydrophobic surface area exacerbates and accelerates protein denaturation upon thermal stress. In fact, we observed a positive association between glycan diversity and lower onset temperature (Figure 6a).^{27,28} Examples of a flipped-out conformation of the CH2 domain, projecting glycans away from the protein surface and exposing them to solvent, have been observed in human IgG4.^{29,30} This may indicate that CH2 configuration can

be impacted by conformational distortion, which can result in a more solvent accessible glycan chains.

We also discerned that plasma stability of payload is construct-dependent. Considering the interaction between carbohydrates and hydrophobic inner patch of the CH2 domain, the drugs attached to the C'E loop are also expected to contact neighboring residues on the inner side of Fc region. Likewise, it is likely that the drug linker covers hydrophobic amino acids and prevents exposure of the denaturation-prone region, especially in the absence of N-glycans contacting the inner region of the CH2 domain. Similar to what is observed for carbohydrate chains, attached payload linkers probably undergo dynamic motion. In some cases such as N297A ADC, the linker payloads might be located within the CH2–CH2 inter-domain cavity in an energetically favorable manner compared to other variants such as CH2-4.16 ADC whose payload linkers are more prone to dynamic fluctuations (Figure 6b). Furthermore, this dynamic motion may be restricted by the presence of N-linked glycans that occupy the inner Fc pocket, resulting in the outstretched conformation of linker payload as seen in the case of CH2-4.20 ADC (Figure 6b). In agreement with this conjecture, thermal destabilization due to elimination of oligosaccharide chains was compensated by introducing the payload linker into the C'E loop within the CH2 domain, whereas this drug-mediated stabilization effect was highly dependent on the conjugation site. However, an exceptional case was noted for the relationship between location of drug and plasma stability of payload. For instance, though CH2-4.19 ADCs showed substantial plasma stability regardless of glycans, introduction of linker payload did not lead to thermal stabilization. It is possible that in CH2-4.19 ADCs, drugs are incapable of filling the CH2 cavity that allows for carbohydrate–aromatic interactions essential for thermal stabilization. However, the drug is stabilized due to the local environment rendering deacetylation unfavorable.

All together, we classified site-specific ADC variants into four categories depending on the position of N-glycans and linked payloads, relative to Fc region (Figure 1). Generally, the glycans extend toward the interstitial space formed by the CH2–CH3 dimer. The glycans on opposite Asn297 residues of each heavy chain interact and maintain the conformation of the Fc domain as well as prevent exposure of hydrophobic patches (Figure 6). The insertion of a non-native peptide to the CH2 domain and shifting glycosylation residue could have negative effects on accommodation of carbohydrate in the inter-domain pocket. It has been reported that shifting the glycosylation site by a single residue can result in altered orientation of oligosaccharides from facing inward between the two Fc domains to facing outward.³¹ In a Class I ADC, it is possible that neither drugs nor glycans are capable of occupying the interstitial space (Figure 1a). For instance, thermal stability and glycan diversity data support the notion that N-glycans in construct CH2-4.10 do not fill the inter-chain cavity. Aglycosylated antibody (CH2-4.10 N299A) undergoes a significant thermal stabilization upon drug attachment. On the other hand, tubulysin in both glycosylated and aglycosylated ADCs undergoes considerable deacetylation. A potential explanation is that though drugs can help maintain native CH2 conformation by filling the inner portion of the CH2 dimer, the acetyl group distant from the conjugation site remains somewhat exposed. A Class II ADC projects N-glycans to solvent-exposed regions, whereas drugs are buried in the inter-chain cavity (Figure 1b). The flexibility of N-linked glycans may facilitate access of conjugated linker payloads to the inter-domain pocket, whereas drugs can interact with residues located

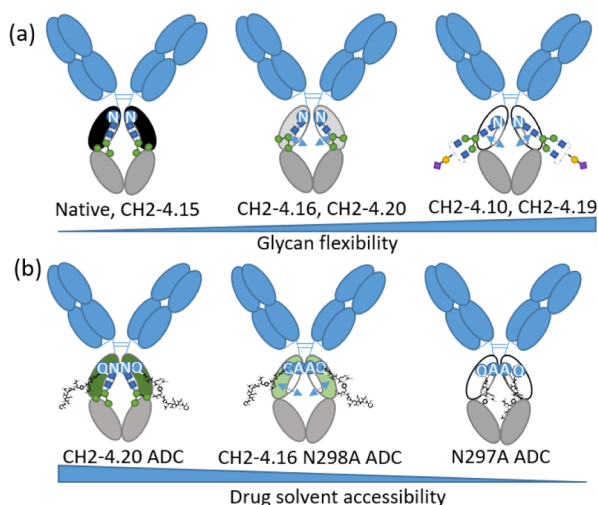


Figure 6. Native antibodies have carbohydrates that interact with neighboring amino acids on the inner side of CH2. White ovals represent a hydrophobic patch in the CH2 domain that is masked by the carbohydrate in native IgG1. (a) Strength of the glycan–CH2 inner patch interaction is altered by the location of the glycosylation site. Variants ordered from least to most dynamic glycans: Native, CH2-4.15 > CH2-4.16, CH2-4.20 > CH2-4.10, CH2-4.19. (b) Solvent accessibility of attached drug is dependent on the location of drug, N-glycans. Representative ADC ordered from most to least exposed drug: CH2-4.20 ADC > CH2-4.16 ADC > N297A ADC.

inside of the CH2 chain. Therefore, the linked payloads are retained in the CH2 domain both in the presence and absence of carbohydrates. Among the ADCs tested in our study, CH2-4.19 falls into this class. In this construct, the drugs can be sequestered in the Fc domain, where a compact folded structure limits access to serum enzymes, therefore the acetyl group is protected in the local environment, whereas this does not permit thermal stabilization. Class III assumes considerable interaction between the carbohydrate chain and inner portion of the CH2 domain. The attached drug's contact with the inner surface of Fc may be hampered because of the competition with glycans, whereas the CH2–CH3 inner pocket can accommodate the drugs in the aglycosylated construct (CH2-4.20, Figure 1c). The fourth case scenario is that the position and orientation of conjugation do not allow the linker payload to fill the CH2–CH3 inter-chain domain, regardless of N-linked glycosylation such as CH2-4.16 (Figure 1d). In this case, the protection of payload from serum protein-mediated metabolism will be compromised, and conjugation of drugs to C'E loop is anticipated to have negligible effects on thermal stabilization of the CH2 domain due to the lack of substantial interactions between protein–drug interfaces.

Engineering of the CH2 domain did not have significantly detrimental impacts on Fc–FcγRs interaction, whereas minor negative effects were noted for genetic variants containing relatively large insertion. This could be explained by the presence of a cavity that can accommodate extra non-native peptide insertion adjacent to the C'E loop. Remarkably, introduction of linker payload was well tolerated with regards to binding to FcγRs. These glycosylated variants can provide a new approach to yield site-specific bTGase-mediated ADCs with preserved Fc–FcγRs interactions. This feature is particularly important for the cases where effector functions are critical or favorable for ADC activity.³

In summary, it was established that both N-glycosylation and conjugation of linker payload to the CH2 domain impact thermal transition profiles and plasma stability of site-specific ADCs. The CH2 domain of the Fc region provides a unique opportunity for site-specific bioconjugation because of the distinct chemical nature of oligosaccharides, availability of chemical and enzymatic methods to remodel the conserved N-linked glycans, and presence of bTGase substrate recognition motif.³² The results of our study demonstrate that genetic engineering of the C'E loop, elimination of sugar chains, and introduction of linker payload combine to yield diverse consequences in chemical and physical stability of site-specific ADCs. The finding emphasizes the importance of careful consideration to achieve the favorable features of therapeutic biologics including thermal properties, glycan homogeneity, and metabolic stability of payload.

EXPERIMENTAL SECTION

Synthesis. Synthesis of tubulysin for bTGase conjugation is described in U.S. patents (US10279049B2).

Expression and Purification of Antibodies. The engineered antibody was produced by transient transfection in mammalian cell expression system. Expi293 cells were used to express the antibodies, grown in Expi293 medium at 37 °C and 8% CO₂ atmosphere in plastic flasks. The expression vectors (pTT5) for the heavy chain and light chain were mixed in OptiMEM, followed by PEI in OptiMEM, and the resulting PEI/DNA complex was incubated at room temperature for 30 min before adding to the cells. 24 h after transfection, Feed B and

VPA were added to the cells and the cells were kept at 37 °C with agitation. After 7 days, the culture supernatant was harvested by filtration using diatomaceous earth as a filter aid. The supernatant was purified with MabSelect SuRe LX resin. Briefly, the cell supernatant was incubated with resin overnight at 4 °C, washed with 10 resin volume of PBS, followed by elution with 4 resin volume of 0.1 M citrate at a pH of 3.5, and immediately neutralized with 1/10 volume of 1 M Tris at a pH of 9. The eluted protein was dialyzed into PBS at a pH of 7.4.

Conjugation. Microbial transglutaminase with double mutations (V65I and Y85F) was used for conjugation. The purified antibodies (~2 mg/mL in 20 mM Tris pH 8 buffer) were reacted with 10-fold molar (per site) excess of the amine donor in the presence of 0.2 M recombinant bTGase per antibody. The reaction was allowed to proceed for 24 h at 37 °C with continuous gentle mixing. Formation of drug conjugates was monitored by mass spectrometric analysis under denaturing conditions. The samples were diluted to 1 mg/mL in 100 mM Tris at a pH of 7.5. 20 μL of sample was reduced by adding 2 μL of 0.5 M TCEP. The samples were analyzed by LC–MS using an Agilent 1290 Infinity UPLC coupled to a 6530 Accurate-Mass Q-TOF mass spectrometer (Agilent, Santa Clara, CA). The analytical column used was a Waters BEH C4 column, 1.7 μm, 2.1 mm × 50 mm held at 60 °C. The mobile phase consisted of 0.1% formic acid in water (A) and 0.1% formic acid in acetonitrile (B). The system was operated at a flow rate of 200 μL/min. The gradient condition was as follows: 0–2 min, held at 27% B; 2–9 min, slow ramp from 27 to 37% B; 9–9.5 min, linear ramp from 37 to 90% B; and 9.5–12.3 min, held at 90% B. The MS settings were as follows: polarity = positive, capillary voltage = 4.2 kV, sample cone = 40 V, source offset = 15 V, source temperature = 140 °C, and desolvation temperature = 325 °C. The data acquisition range was 900–3200 *m/z*. Deconvolution was performed using Agilent MassHunter WalkUp Software.

Differential Scanning Calorimetry. DSC thermal analysis of parental antibodies and conjugated products was performed using the Malvern MicroCal VP-Capillary DSC (Malvern Instruments, Westborough, MA, USA). All samples were analyzed at a protein concentration of 1.0 mg/mL in PBS at a pH of 7.4. 550 μL of samples and buffer were added in a polypropylene round-bottom 96-well plate (Microtiter Analytical Supplies Inc., Suwanee, GA, USA), covered with a MicroMat clear silicone mat (Thermo Scientific, Waltham, MA, USA) and placed in a temperature-controlled storage box at 4 °C for the duration of analysis. The excess heat capacity was monitored across a scan range of 15–95 °C at a heating rate of 60 °C/h. Data were buffer subtracted and baseline corrected in MicroCal Origin 7.0 software (Malvern Instruments, Westborough, MA, USA) and the temperature corresponding to the apex of endothermic transitions was defined as apparent *T_m*.

Evaluation of ADC Stability in SCID Mouse Serum. ADCs were diluted to a target concentration of 50 μg/mL in 500 μL of SCID mouse serum and incubated at 37 °C. From the incubating sample plate, 80 μL of serum samples were collected and immediately frozen on days 0, 1, 2, and 3. All the ADCs were extracted from serum using the dual affinity capture method and analyzed by LC–HRMS as previously reported.²⁴ In brief, the ADCs were captured from serum using a generic anti-human F(ab')₂ reagent. The immobilized HC-Fc conjugated ADCs were digested with IdeS (aglycosylated ADCs) or IdeS + PNGase F (N-glycan ADCs) to release the deglycosylated Fc fragment. The beads were discarded and Fc present in the digestion mixture is further captured by addition of a second set

of beads coated with anti-human Fc capture reagent.²⁴ The MS data were analyzed following deconvolution using Intact Mass software (v3.6, Protein Metrics, Inc.) The relative peak intensities of parent (ADC fragment with acetyl payload) and catabolite (ADC fragment with deacetyl payload) were used to determine the relative percent deacetylation.

Surface Plasmon Resonance Analysis. The model of the protein and small molecule was generated and energy minimization was conducted using Molecular Operating Environment (MOE) tool. The model demonstrated feasibility of proposed conformation. The binding experiments were performed on a Biacore 8K instrument (Cytiva, Marlborough, MA) at 25 °C in running buffer consisting of 10 mM sodium phosphate, 130 mM sodium chloride, and 0.05% Tween 20, and pH = 7.2 (PBS-T). Diluted antibody samples were injected over a Protein A sensor chip surface (Cytiva) for 30 s at 30 μ L/min to an average capture level of about 250RU. Fc γ R₁ were then injected at 30 μ L/min at concentrations of 1.4, 4.1, 12.4, 37, 111, 333, and 10,000 nM for 120 s, followed by 120 s of dissociation in running buffer. The protein A surface was regenerated between cycles by injecting two 15 s pulses of 10 mM glycine at a pH of 1.5 at 3 μ L/min. Sensorgram data were double referenced and fitted to both 1:1 Langmuir model and/or steady-state affinity model using Biacore Insight Evaluation Software V3.0.12 to determine the equilibrium dissociation constants.

HILIC-FLR of Labeled N-Glycans. Labeled N-glycans were analyzed via HILIC-FLR with a Waters ACQUITY UPLC H-Class Bio system (Milford, MA). Separations were performed using an ACQUITY UPLC Glycan BEH Amide column (130 Å, 1.7 μ m, 2.1 \times 150 mm; Waters Corporation). By using a column temperature of 60 °C, over the course of 35 min, a gradient starting at 25% 50 mM ammonium formate in Milli-Q water at pH = 4.4 (mobile phase A), 10 \times mobile phase concentrate was reequilibrated for 7.4 min under these conditions for a total run time of 55 min. Ten microliters of sample was injected per run using a stainless-steel needle. All wash lines (sample manager wash, sample manager purge, and seal wash) used 70% acetonitrile. Eluting N-glycans were detected via FLR (excitation 265 nm, emission 425 nm) at a 20 Hz sampling rate. Glycan peaks were identified based on retention time comparisons to Waters RFMS-labeled reference standards.

■ ASSOCIATED CONTENT

SI Supporting Information

The Supporting Information is available free of charge at <https://pubs.acs.org/doi/10.1021/acs.bioconjchem.1c00572>.

Supplemental methods on in vitro cytotoxicity assay, antibody deglycosylation, and HTP expression and purification and supplemental results on expression yield of genetic variants, list of MMAE ADCs, stability of MMAE ADCs, cell killing IC₅₀ of tubulysin and MMAE ADCs, glycan component of engineered antibodies, and binding affinities for the Fc γ receptors (PDF)

■ AUTHOR INFORMATION

Corresponding Authors

Sayumi Yamazoe – Discovery Biotherapeutics, Bristol-Myers Squibb, Redwood City, California 94063, United States;

orcid.org/0000-0002-2169-7674;

Email: Sayumi.yamazoe@bms.com

Pavel Strop – Discovery Biotherapeutics, Bristol-Myers Squibb, Redwood City, California 94063, United States; Biologics

Discovery, Tallac Therapeutics, Burlingame, California 94010, United States; Email: pavel@tallactx.com

Authors

Srikanth Kotapati – Discovery Biotherapeutics, Bristol-Myers Squibb, Redwood City, California 94063, United States;

orcid.org/0000-0003-2302-5350

Jason M. Hogan – Discovery Biotherapeutics, Bristol-Myers Squibb, Redwood City, California 94063, United States

Sean M. West – Discovery Biotherapeutics, Bristol-Myers Squibb, Redwood City, California 94063, United States

Xiaodi A. Deng – Dren Bio, Redwood City, California 94063, United States

SJ Diong – Discovery Biotherapeutics, Bristol-Myers Squibb, Redwood City, California 94063, United States

Jaren Arbanas – Discovery Biotherapeutics, Bristol-Myers Squibb, Princeton, New Jersey 08543, United States

Thien Anh Nguyen – Discovery Biotherapeutics, Bristol-Myers Squibb, Redwood City, California 94063, United States

Aarti Jashnani – Discovery Biotherapeutics, Bristol-Myers Squibb, Redwood City, California 94063, United States;

orcid.org/0000-0002-8563-0452

Diksha Gupta – SCIEX, Fremont, California 94538, United States

Arvind Rajpal – Large Molecule Drug Discovery, Genentech, South San Francisco, California 94080, United States

Gavin Dollinger – Discovery Biotherapeutics, Bristol-Myers Squibb, Redwood City, California 94063, United States

Complete contact information is available at:

<https://pubs.acs.org/doi/10.1021/acs.bioconjchem.1c00572>

Notes

The authors declare no competing financial interest.

■ ACKNOWLEDGMENTS

We thank Caleb Cassidy Amstutz, Christine Bee, and Andrew Drake for technical assistance.

■ REFERENCES

- (1) Lehar, S. M.; Pillow, T.; Xu, M.; Staben, L.; Kajihara, K. K.; Vandlen, R.; DePalatis, L.; Raab, H.; Hazenbos, W. L.; Hiroshi Morisaki, J.; et al. Novel antibody-antibiotic conjugate eliminates intracellular *S. aureus*. *Nature* **2015**, *527*, 323–328.
- (2) Kreutz, M.; Giquel, B.; Hu, Q.; Abuknesh, R.; Uematsu, S.; Akira, S.; Nestle, F. O.; Diebold, S. S. Antibody-antigen-adjuvant conjugates enable co-delivery of antigen and adjuvant to dendritic cells in cis but only have partial targeting specificity. *PLoS One* **2012**, *7*, No. e40208.
- (3) Gadd, A. J. R.; Greco, F.; Cobb, A. J. A.; Edwards, A. D. Targeted Activation of Toll-Like Receptors: Conjugation of a Toll-Like Receptor 7 Agonist to a Monoclonal Antibody Maintains Antigen Binding and Specificity. *Bioconjugate Chem.* **2015**, *26*, 1743–1752.
- (4) Buecheler, J. W.; Winzer, M.; Weber, C.; Gieseler, H. Alteration of Physicochemical Properties for Antibody-Drug Conjugates and Their Impact on Stability. *J. Pharm. Sci.* **2020**, *109*, 161–168.
- (5) Adem, Y. T.; Schwarz, K. A.; Duenas, E.; Patapoff, T. W.; Galush, W. J.; Esue, O. Auristatin antibody drug conjugate physical instability and the role of drug payload. *Bioconjugate Chem.* **2014**, *25*, 656–664.
- (6) Deisenhofer, J. Crystallographic refinement and atomic models of a human Fc fragment and its complex with fragment B of protein A from *Staphylococcus aureus* at 2.9- and 2.8-Å resolution. *Biochemistry* **1981**, *20*, 2361–2370.
- (7) Jain, N.; Smith, S. W.; Ghone, S.; Tomczuk, B. Current ADC Linker Chemistry. *Pharm. Res.* **2015**, *32*, 3526–3540.

- (8) Beckley, N. S.; Lazzareschi, K. P.; Chih, H.-W.; Sharma, V. K.; Flores, H. L. Investigation into temperature-induced aggregation of an antibody drug conjugate. *Bioconjugate Chem.* **2013**, *24*, 1674–1683.
- (9) Adhikari, P.; Zacharias, N.; Ohri, R.; Sadowsky, J. Site-Specific Conjugation to Cys-Engineered THIOMAB Antibodies. *Methods Mol. Biol.* **2020**, *2078*, 51–69.
- (10) Axup, J. Y.; Bajjuri, K. M.; Ritland, M.; Hutchins, B. M.; Kim, C. H.; Kazane, S. A.; Halder, R.; Forsyth, J. S.; Santidrian, A. F.; Stafin, K.; et al. Synthesis of site-specific antibody-drug conjugates using unnatural amino acids. *Proc. Natl. Acad. Sci. U.S.A.* **2012**, *109*, 16101–16106.
- (11) Tian, F.; Lu, Y.; Manibusan, A.; Sellers, A.; Tran, H.; Sun, Y.; Phuong, T.; Barnett, R.; Hehli, B.; Song, F.; et al. A general approach to site-specific antibody drug conjugates. *Proc. Natl. Acad. Sci. U.S.A.* **2014**, *111*, 1766–1771.
- (12) Strop, P.; Liu, S.-H.; Dorywalska, M.; Delaria, K.; Dushin, R. G.; Tran, T.-T.; Ho, W.-H.; Farias, S.; Casas, M. G.; Abdiche, Y.; et al. Location matters: site of conjugation modulates stability and pharmacokinetics of antibody drug conjugates. *Chem. Biol.* **2013**, *20*, 161–167.
- (13) Tumej, L. N.; Li, F.; Rago, B.; Han, X.; Loganzo, F.; Musto, S.; Graziani, E. I.; Puthenveetil, S.; Casavant, J.; Marquette, K.; et al. Site Selection: a Case Study in the Identification of Optimal Cysteine Engineered Antibody Drug Conjugates. *AAPS J.* **2017**, *19*, 1123–1135.
- (14) Dickgiesser, S.; Rieker, M.; Mueller-Pompalla, D.; Schroter, C.; Tonillo, J.; Warszawski, S.; Raab-Westphal, S.; Kuhn, S.; Knehans, T.; Konning, D.; et al. Site-Specific Conjugation of Native Antibodies Using Engineered Microbial Transglutaminases. *Bioconjugate Chem.* **2020**, *31*, 1070.
- (15) Liu, H.; Gaza-Bulsecu, G.; Xiang, T.; Chumsae, C. Structural effect of deglycosylation and methionine oxidation on a recombinant monoclonal antibody. *Mol. Immunol.* **2008**, *45*, 701–708.
- (16) Sussman, D.; Westendorf, L.; Meyer, D. W.; Leiske, C. I.; Anderson, M.; Okeley, N. M.; Alley, S. C.; Lyon, R.; Sanderson, R. J.; Carter, P. J.; et al. Engineered cysteine antibodies: an improved antibody-drug conjugate platform with a novel mechanism of drug-linker stability. *Protein Eng. Des. Sel.* **2018**, *31*, 47–54.
- (17) Jeger, S.; Zimmermann, K.; Blanc, A.; Grünberg, J.; Honer, M.; Hunziker, P.; Struthers, H.; Schibli, R. Site-specific and stoichiometric modification of antibodies by bacterial transglutaminase. *Angew. Chem., Int. Ed.* **2010**, *49*, 9995–9997.
- (18) Yamazoe, S.; Hogan, J.; West, S.; Deng, X.; Kotapati, S.; Shao, X.; Holder, P.; Lamba, V.; Huber, M.; Qiang, C.; et al. High-Throughput Platform to Identify Antibody Conjugation Sites from Antibody-Drug Conjugate Libraries. *Bioconjugate Chem.* **2020**, *31*, 1199.
- (19) Yokoyama, K.; Utsumi, H.; Nakamura, T.; Ogaya, D.; Shimba, N.; Suzuki, E.; Taguchi, S. Screening for improved activity of a transglutaminase from *Streptomyces mobaraensis* created by a novel rational mutagenesis and random mutagenesis. *Appl. Microbiol. Biotechnol.* **2010**, *87*, 2087–2096.
- (20) Zheng, K.; Yarmarkovich, M.; Bantog, C.; Bayer, R.; Patapoff, T. W. Influence of glycosylation pattern on the molecular properties of monoclonal antibodies. *mAbs* **2014**, *6*, 649–658.
- (21) Ionescu, R. M.; Vlasak, J.; Price, C.; Kirchmeier, M. Contribution of variable domains to the stability of humanized IgG1 monoclonal antibodies. *J. Pharm. Sci.* **2008**, *97*, 1414–1426.
- (22) Ghirlando, R.; Lund, J.; Goodall, M.; Jefferis, R. Glycosylation of human IgG-Fc: influences on structure revealed by differential scanning micro-calorimetry. *Immunol. Lett.* **1999**, *68*, 47–52.
- (23) Zheng, K.; Bantog, C.; Bayer, R. The impact of glycosylation on monoclonal antibody conformation and stability. *mAbs* **2011**, *3*, 568–576.
- (24) Kotapati, S.; Passmore, D.; Yamazoe, S.; Sanku, R. K. K.; Cong, Q.; Poudel, Y. B.; Chowdari, N. S.; Gangwar, S.; Rao, C.; Rangan, V. S.; et al. Universal Affinity Capture Liquid Chromatography-Mass Spectrometry Assay for Evaluation of Biotransformation of Site-Specific Antibody Drug Conjugates in Preclinical Studies. *Anal. Chem.* **2020**, *92*, 2065–2073.
- (25) Yanaka, S.; Yogo, R.; Inoue, R.; Sugiyama, M.; Itoh, S. G.; Okumura, H.; Miyanoiri, Y.; Yagi, H.; Satoh, T.; Yamaguchi, T.; et al. Dynamic Views of the Fc Region of Immunoglobulin G Provided by Experimental and Computational Observations. *Antibodies* **2019**, *8*, 39.
- (26) Chen, W.; Kong, L.; Connelly, S.; Dendle, J. M.; Liu, Y.; Wilson, I. A.; Powers, E. T.; Kelly, J. W. Stabilizing the CH2 Domain of an Antibody by Engineering in an Enhanced Aromatic Sequon. *ACS Chem. Biol.* **2016**, *11*, 1852–1861.
- (27) Remesh, S. G.; Armstrong, A. A.; Mahan, A. D.; Luo, J.; Hammel, M. Conformational Plasticity of the Immunoglobulin Fc Domain in Solution. *Structure* **2018**, *26*, 1007–1014.
- (28) Buck, P. M.; Kumar, S.; Singh, S. K. Consequences of glycan truncation on Fc structural integrity. *mAbs* **2013**, *5*, 904–916.
- (29) Scapin, G.; Yang, X.; Prosis, W. W.; McCoy, M.; Reichert, P.; Johnston, J. M.; Kashi, R. S.; Strickland, C. Structure of full-length human anti-PD1 therapeutic IgG4 antibody pembrolizumab. *Nat. Struct. Mol. Biol.* **2015**, *22*, 953–958.
- (30) Tischenko, V. M.; Zav'yalov, V. P.; Ryazantsev, S. N. Human myeloma IgG4 reveals relatively rigid asymmetric Y-like structure with different conformational stability of CH2 domains. *Mol. Immunol.* **2017**, *92*, 199–210.
- (31) Zhou, Q.; Jaworski, J.; Zhou, Y.; Valente, D.; Cotton, J.; Honey, D.; Boudanova, E.; Beninga, J.; Rao, E.; Wei, R.; et al. Engineered Fc-glycosylation switch to eliminate antibody effector function. *mAbs* **2020**, *12*, 1814583.
- (32) Qasba, P. K. Glycans of Antibodies as a Specific Site for Drug Conjugation Using Glycosyltransferases. *Bioconjugate Chem.* **2015**, *26*, 2170–2175.